



# Design and control of a wearable and force-controllable hand exoskeleton system<sup>☆</sup>



Inseong Jo, Joonbum Bae\*

Department of Mechanical Engineering, UNIST, Ulsan, Korea

## ARTICLE INFO

### Article history:

Received 4 January 2016

Revised 1 November 2016

Accepted 3 December 2016

### Keywords:

Hand exoskeleton

Wearable structure

Force control

Series elastic actuator (SEA) mechanism

## ABSTRACT

In this paper, a wearable and force-controllable hand exoskeleton system is proposed. In order to apply force feedback to the fingertip while allowing natural finger motions, the exoskeleton linkage structure with three degrees of freedom (DOFs) was designed, which was inspired by the muscular skeletal structure of the finger. Kinematic performance of the proposed linkage structure was verified by comparing with functional range of motion (ROM) which is required for activities in daily living. As an actuating system, a series elastic actuator (SEA) mechanism, which consisted of a small linear motor, a manually designed motor driver, a spring and potentiometers, was applied. Friction of the motor was identified and compensated to obtain a linearized model of the actuating system. Using a linear quadratic (LQ) tuned proportional-derivative (PD) controller and a disturbance observer (DOB), the proposed actuator module could generate the desired force accurately even with arbitrary finger movement. The performance of force transmission through linkage structure was verified by simulation and experiments. The proposed exoskeleton structure, actuator modules and control algorithms were integrated as a wearable and force-controllable hand exoskeleton system that could deliver force to the fingertips for flexion/extension motions.

© 2016 Elsevier Ltd. All rights reserved.

## 1. Introduction

Exoskeleton systems have been actively researched for rehabilitation and power augmentation [4,17,20,25,26]. Among the research areas, interacting with virtual reality using an exoskeleton interface is one of the most promising applications of exoskeleton systems. Many related studies on virtual reality have focused on head-mounted display (HMD) systems or tactile sensors [13], which in turn have accelerated the need for wearable interaction systems.

The hand is the richest source of tactile feedback, significant amounts of data are obtained through the hand. We receive force feedback and determine the mechanical properties of objects while manipulating the objects by using the hand. Therefore, development of the wearable force feedback systems for the hand is essential for the interaction with virtual environment.

In this paper, a wearable and force-controllable hand exoskeleton system is proposed as a motor-actuated exoskeleton system,

which focuses on transmitting the desired force to the fingertips. Inspired by the muscular skeletal structure of the hand, the linkage structure of the hand exoskeleton was designed, which allows three degrees of freedom (DOFs) and large range of motions (ROM) of each finger. A series elastic actuator (SEA) mechanism with an electric motor was applied to the actuator module to satisfy both requirements of compact size and force mode control. In the SEA mechanism, the spring acts as a force sensor, which decreases size and weight of the actuator. Also, a proportional-derivative (PD) controller was applied with a robust controller, disturbance observer (DOB), to achieve the force control even with user's finger motions. By integrating the exoskeleton structure, actuator modules, and control algorithms, a wearable and force-controllable hand exoskeleton system was developed.

The remainder of this paper is organized as follows. In Section 2, previous researches about wearable devices for the hand are reviewed. The design of the proposed hand exoskeleton structure is presented and analyzed in Section 3. The design and control algorithms of the compact and force-controllable actuator modules are discussed in Sections 4 and 5. The implementation of the proposed system is given in Section 6, and conclusions and future work are presented in Section 7.

\* This paper was recommended for publication by Associate Editor Vicente Feliu.

<sup>☆</sup> Corresponding author.

E-mail addresses: [isjo@unist.ac.kr](mailto:isjo@unist.ac.kr) (I. Jo), [jbbae@unist.ac.kr](mailto:jbbae@unist.ac.kr) (J. Bae).

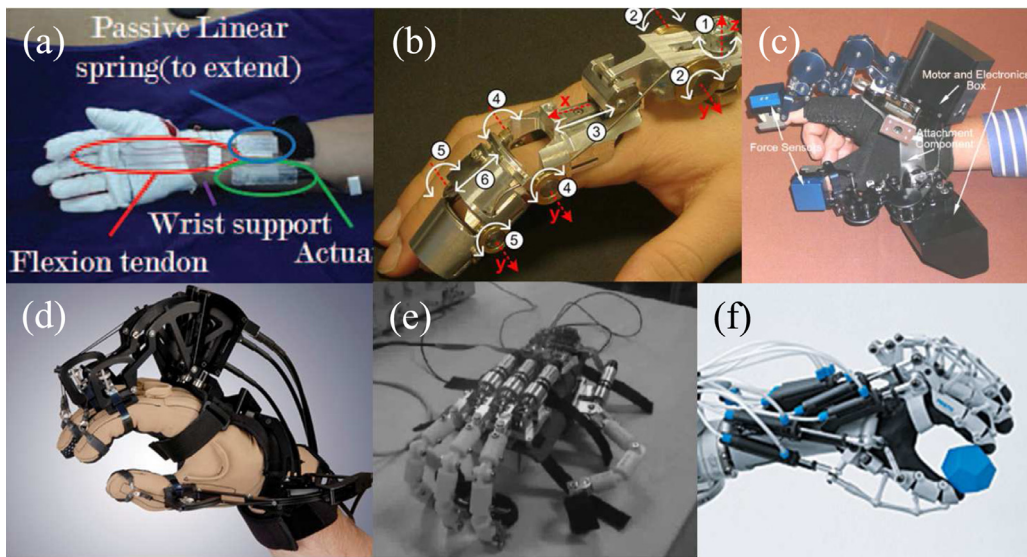


**Fig. 1.** Previously developed wearable interaction systems for the hand [6–9,11,12].

## 2. State of the arts: wearable interaction systems for the hand

There have been many attempts to develop wearable interaction systems for the hand. Previously developed systems can be categorized into (1) cable-driven glove systems, (2) cable-driven frame systems, and (3) exoskeleton systems by their structures and actuating mechanisms.

As a cable-driven glove system, Exo-Glove [Fig. 1(a)] was developed [11]. It is an assistive glove for disable people. The assisting force produced by an electric motor is applied via cables. Because this system does not have a rigid frame, it is light and easy to wear. However, applying the force at the specific location without frames is difficult and precise tension control is hard to be realized without the tension sensing mechanism.

Fig. 1(b)–(d) shows examples of the cable-driven frame systems, which have more rigid parts than the cable-glove configuration. The frames in the cable-driven frame systems support the finger and guide the cable. HANDEXOS [Fig. 1(b)] has cable pulleys positioned at either side of each joint to transmit the generated torque [6]. However, the pulleys make it difficult for adjacent fingers to be close sufficiently, prohibiting natural finger motion. The hand exoskeleton system from PERCRO Laboratory [Fig. 1(c)] uses cable modules driven by motors [9]. In this system, three motors are used for each finger to change the direction and magnitude of the applied force; however, the system as a whole is large and cumbersome. CyberGrasp (Fig. 1(d)) was developed as a cable-driven frame system using one motor for each finger [7]; in this system, the interference problem is minimized by putting the cable structure on the upper side of fingers. However, the system is large due to the required parts for the cable mechanism.

The hand exoskeleton system, which utilized one active revolute joint for each finger, was developed (Fig. 1(e)) [12]. It satisfies finger workspaces with a simple structure, but the whole system is quite big due to the space between the hand and exoskeleton structure for finger motions. FESTO developed a hand exoskeleton as a master-slave system with pneumatic actuators (Fig. 1(f)) [8]. It shows smooth motion, but the required peripherals for the pneumatic actuators restrict its mobility.

The exoskeleton system may have the most complicated structure; however, the ability in delivering force to the fingers may be the best among the above mentioned systems. To date, the simple linkage structure, which guarantees sufficient motion range and force transmission to the fingers, has yet to be fully exploited. A

compact and force-controllable actuator module is also required to deliver interaction forces to the fingers. In this paper, a hand exoskeleton structure inspired by a muscular skeletal system of the hand and compact and force-controllable actuator modules are proposed for a wearable and force-controllable hand exoskeleton system.

## 3. Design of a linkage structure for the hand exoskeleton

### 3.1. Anatomy of the hand

The human hand is moved by 19 bones, 19 joints and 29 muscles [15]. 14 phalanx bones of the fingers and 5 metacarpal bones meet at 14 joints, and these make fingers move in various directions. The main movements of the finger are flexion and extension at three rotational joints (blue dashed circles in Fig. 2): metacarpophalangeal, proximal phalangeal and distal phalangeal joints. Therefore, the exoskeleton structure should be designed for guaranteeing natural flexion/extension motions with three DOFs. Besides, the system is developed for transmitting interactive force to the finger with respect to grasping virtual objects so that it should provide resistive forces to the finger in extension direction. Thus, the basic structure was designed as an upward structure (red arrows beside joints in Fig. 2) inspired by the extensor mechanism.

### 3.2. Design of an exoskeleton structure

The structure with three DOFs in flexion/extension direction was designed for guaranteeing natural finger motions while interacting with virtual objects. Adduction and abduction motions of the finger are also important, especially in case of the thumb, but the flexion and extension were mainly considered in this paper for the simple structure.

The interactive forces are applied to the finger in extension direction with respect to grasping objects. In particular, the most interactions between the finger and objects are occurred at the bottom side of the fingertip. Thus, the connecting part for the fingertip was located at the bottom side.

To deliver force to the fingertips for the flexion and extension motions, several linkage structures were discussed. Fig. 3 shows feasible designs of the hand exoskeleton. Inspired by the extensor mechanism in Fig. 2, the exoskeleton structure was designed to contact the finger at the three points (grey line-patterned parts

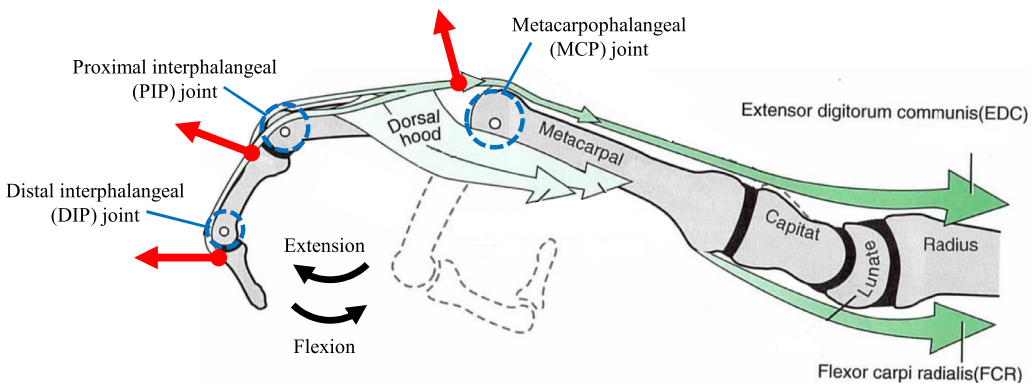


**Fig. 2.** Anatomy of the finger (edited from [15]).

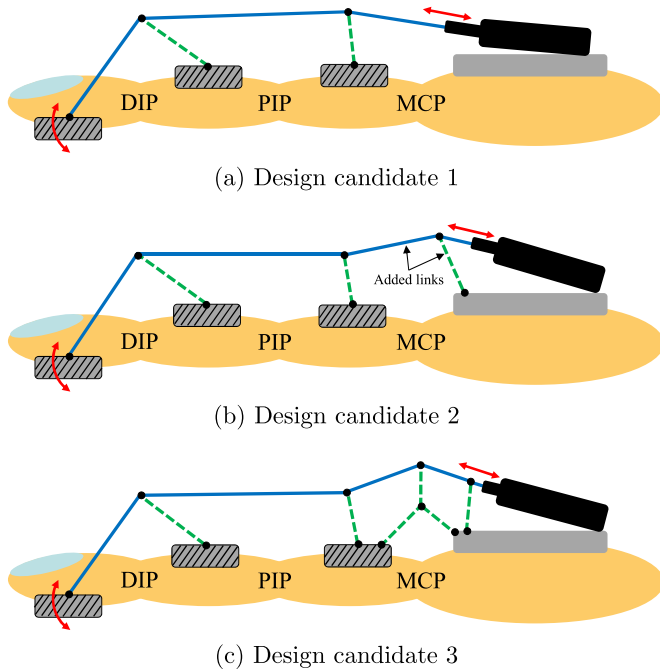


**Fig. 3.** Design candidates for the linkage structure.

in the figure), and the structures were built above the finger to avoid interference between adjacent fingers. The blue links (solid lines) deliver the generated force to the fingertip, and the green links (dashed lines) mainly support the structure from the finger. Also, the actuators were located at the dorsal side of the hand, as the extensor muscles did, for the compact size of the system.

In the first design shown in Fig. 3(a), the blue links connect the supporting links and the actuator. It may be the simplest design, but it has only two DOFs, which is not enough for natural movement of the finger. By adding more links at the last linkage as shown in Fig. 3(b), DOFs of the structure are increased to three. However, the range of motion of the structure is easily restricted by the length of the last two links as shown in Fig. 4(a). The last linkage in design candidate 2 was divided to have three loops as shown in Fig. 3(c). The finger postures were same in design candidate 2 and 3 in Fig. 4. Flexion of PIP and DIP joint in both design candidates is impossible from the shown posture because of the interference between links. The MCP joint flexion in candidate 2 was restricted due to short lengths of links. On the other hand, in candidate 3, the four-bar linkage composed of the finger and links guarantees the space for MCP joint flexion and the finger can flex more from the shown posture. This structure allows more ROM as shown in Fig. 4(b) while maintaining three DOFs. By adopting this

design, the whole linkage structure of one finger was designed as shown in Fig. 5.

### 3.3. Kinematic analysis of the proposed linkage structure

The user wants to move his/her finger naturally with the proposed exoskeleton but the some postures may be impossible due to the interferences between links and insufficient link lengths. Therefore, the ROM of the proposed linkage structure was kinematically analyzed by subdividing the structure into several four or five-bar linkages as shown in Fig. 6: two four-bar linkages and three five-bar linkages. The numbers inside of each linkage in Fig. 6(b) represent the number of links in the linkage.

Given angles of MCP, PIP and DIP joints, the position of each link was calculated sequentially by applying kinematic equations of four and five-bar linkages from the MCP joint side. The length variables and angle variables of the proposed links for kinematic analysis are shown in Fig. 7(a) and (b), respectively. The  $x$ -axis was set to parallel with the dorsum of hand and the point 4 was set as the origin for investigating the fingertip position. The positions of the MCP, PIP and DIP joints were point 7, 11, and 14, respectively and point 17 was the position of the fingertip. The angle  $\alpha$  in Fig. 7(b) is the angle between  $x$ -axis and line  $l_{24}$  at the exoskeleton part and the angle  $\beta$  is the angle between  $x$ -axis and line  $l_7$  connecting point 4 and 7 (MCP joint). The exoskeleton device is always located at the same position on the dorsum of the hand, accordingly, the angles  $\alpha$  and  $\beta$  were assumed constant. The  $\theta_1$ ,  $\theta_2$  and  $\theta_3$  are the MCP, PIP and DIP joint angles determined by the human finger posture.

The functional ROM is the finger motion range required to perform activities of daily living such as pinch, grasp, key grip and so on, and the normal ROM is the minimum and maximum angle where each joint can reach [10]. Therefore, the ranges of joint angles were determined by functional ROM because the exoskeleton was used for manipulating objects and conducting task in virtual reality. The normal ROM were also compared with the possible ROM of each joint by the proposed exoskeleton structure in later part. The parameters for kinematic analysis were summarized in Table 1.

By predefined angles  $\alpha$  and  $\beta$ , the point 1, 4 and 7 are determined. Also, the positions of finger joints and fingertip (pt 11, 14, 17) are identified by the finger joint angles  $\theta_1$ ,  $\theta_2$  and  $\theta_3$ . The position of the fingertip is calculated by following equations:

$$\begin{aligned} \vec{P}_{17} &= \vec{l}_7 + \vec{l}_{10} + \vec{l}_{15} + \vec{l}_{23} \\ &= l_7 T(-\beta) + l_{10} T(-\theta_1) + l_{15} T(-\theta_1 - \theta_2) \\ &\quad + l_{23} T(-\theta_1 - \theta_2 - \theta_3) \end{aligned} \quad (1)$$

where  $T(\theta) = [\cos(\theta) \quad \sin(\theta); \quad -\sin(\theta) \quad \cos(\theta)]$ . The positions of point 8, 9, 12 and 16 are also determined automatically because

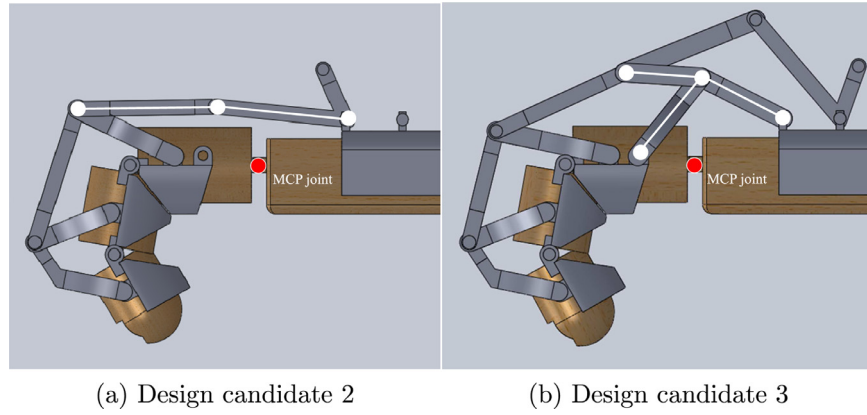


Fig. 4. Comparison of ROM of the design candidates.

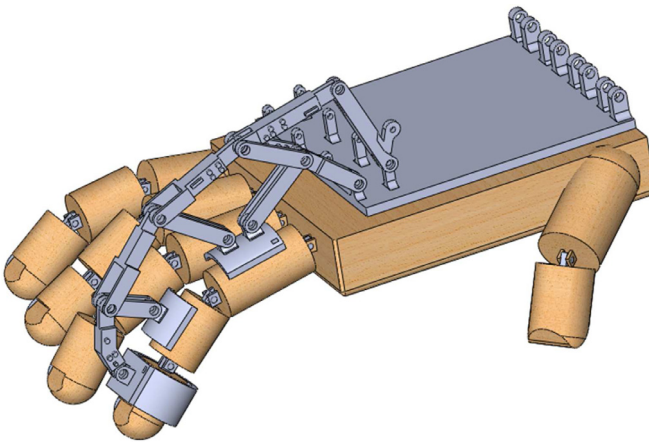


Fig. 5. Final design of the proposed linkage structure (one finger case).

**Table 1**  
Parameters for kinematic analysis.

	Predefined angles ( $^{\circ}$ )	$\alpha, \beta$
	Link lengths (mm)	$l$
Position		
Origin	pt 4	
MCP joint	pt 7	
PIP joint	pt 11	
DIP joint	pt 14	
fingertip	pt 17	
Range of finger joint angles	MCP ( $^{\circ}$ )	0 ~ 73
	PIP ( $^{\circ}$ )	0 ~ 86
	DIP ( $^{\circ}$ )	0 ~ 57

they are joints on the attached parts to the finger phalanges. Other joint positions will be obtained by analyzing the four- or five-bar linkages.

To describe the proposed exoskeleton structure easily, the order of linkage was written inside of the linkage shown in Fig. 7(b).

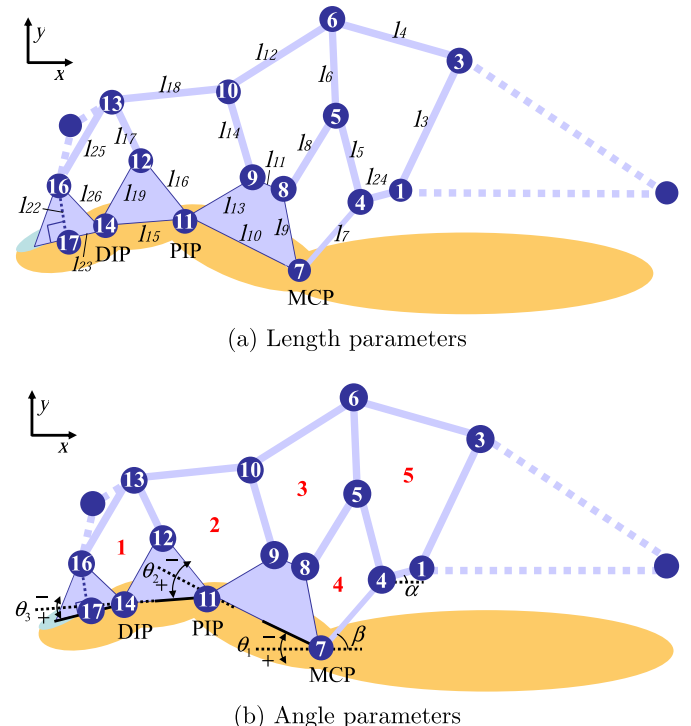


Fig. 7. Parameters for kinematic analysis.

The leftmost linkage 1 is a four-bar linkage that has 1 DOF and all joint positions except point 13 were investigated before. The analysis equations for the four-bar linkage are used to find out the point 13 position in linkage 1. Fig. 8 represents the schematic of linkage 1. The  $x' - y'$  plane is tilted with the angle  $\delta$  from the  $x - y$  plane and the angle  $\delta$  can be calculated from positions of point 12 and 14 investigated before.  $\varphi$  is the included angle between links connecting the point 12, 14 and 16 and it is calculated using law of

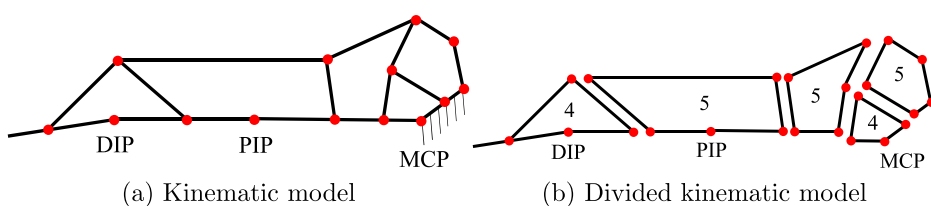


Fig. 6. Kinematic model of the proposed structure.

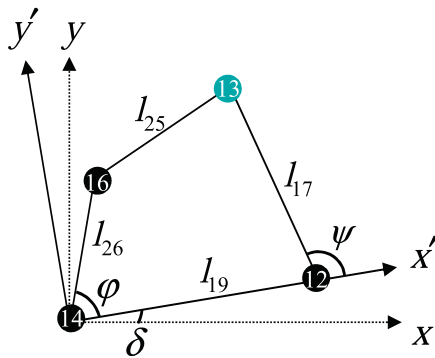


Fig. 8. Linkage 1.

cosines:

$$\varphi = \arccos \left( \frac{l_{26}^2 + l_{19}^2 - \|\vec{P}_{16} - \vec{P}_{12}\|^2}{2l_{26}l_{19}} \right) \quad (2)$$

Suppose  $\varphi$  is the input angle, then the joint position of point 13 is calculated as follows [21]:

$$(\vec{P}_{16} - \vec{P}_{13}) \cdot (\vec{P}_{16} - \vec{P}_{13}) - l_{25}^2 = 0 \quad (3)$$

where  $\vec{P}_{16} = l_{26}T(\varphi)$  and  $\vec{P}_{13} = l_{19}[1 \ 0]^T + l_{17}T(\psi)$  in the  $x' - y'$  plane. It is rewritten as follows:

$$\mathbf{A}(\varphi) \cos \psi - \mathbf{B}(\varphi) \sin \psi + \mathbf{C}(\varphi) = 0 \quad (4)$$

where

$$\mathbf{A}(\varphi) = 2l_{17}l_{19} - 2l_{17}l_{26} \cos \varphi \quad (5)$$

$$\mathbf{B}(\varphi) = 2l_{17}l_{26} \sin \varphi \quad (6)$$

$$\mathbf{C}(\varphi) = l_{26}^2 + l_{17}^2 + l_{19}^2 - l_{25}^2 - 2l_{26}l_{19} \cos \varphi \quad (7)$$

Then, the output angle,  $\psi$ , is determined by the input angle,  $\varphi$  using following equation:

$$\psi = \arctan \left( \frac{\mathbf{B}(\varphi)}{\mathbf{A}(\varphi)} \right) \pm \arccos \left( -\frac{\mathbf{C}(\varphi)}{\sqrt{\mathbf{A}(\varphi)^2 + \mathbf{B}(\varphi)^2}} \right) \quad (8)$$

The position of point 13 can be expressed as follows:

$$\vec{P}_{13} = \vec{P}_{12} + l_{17}T(\delta + \psi) \quad (9)$$

Therefore, all joint positions in linkage 1 were investigated through the four-bar linkage analysis. The linkage 4 is also a four-bar linkage with 1 DOF and all positions in linkage 4 can be defined by above equations. In case of the five-bar linkage, it has 2 DOFs so that requires two input angles to find out the unknown joint positions. As shown in Fig. 9, the linkage 2 is a five-bar linkage that has two input angles  $\phi$  and  $\omega$ , and the position of point 10 should be identified. The  $x'' - y''$  plane is also rotated with the angle  $\nu$  compared with the  $x-y$  plane and the angle  $\nu$  is calculated easily by positions of point 11 and 12. The input angles  $\phi$  and  $\omega$  are obtained by using the law of cosines with similar ways to calculate the angle  $\varphi$  in linkage 1. The position of point 10 can be expressed as follows [23]:

$$\vec{P}_{10} = \vec{P}_{13} + l_{18}T(\psi_1 + \psi_2) \quad (10)$$

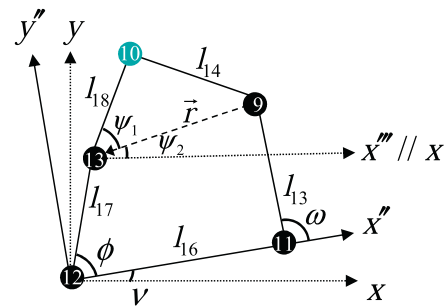


Fig. 9. Linkage 2.

The vector  $\mathbf{r}$  connecting point 9 to point 13 is investigated for calculating  $\psi_1$  and  $\psi_2$ :

$$\mathbf{r} = \vec{P}_9 - \vec{P}_{13} = \vec{l}_{16} + \vec{l}_{13} - \vec{l}_{17} = l_{16}T(\nu) + l_{13}T(\nu + \omega) - l_{17}T(\nu + \phi) \quad (11)$$

By using the connecting vector  $\mathbf{r}$ ,  $\psi_1$  and  $\psi_2$  are obtained by following equations:

$$\psi_1 = \arccos \left( \frac{l_{18}^2 + \|\mathbf{r}\|^2 - l_{14}^2}{2l_{18}\|\mathbf{r}\|} \right) \quad (12)$$

$$\psi_2 = \arccos \left( \frac{\mathbf{r} \cdot [1 \ 0]^T}{\|\mathbf{r}\|} \right) \quad (13)$$

Therefore, the point 10 position with  $\psi_1$  and  $\psi_2$  is determined and the all joint positions in linkage 2 are obtained kinematically. In a similar way, the linkage 3 and 5 that are five-bar linkage are also investigated. Finally, all link and joint positions were investigated kinematically. Among investigated human finger postures, however, some finger postures are excluded due to the interference between links and insufficient link lengths in the proposed exoskeleton structure.

The possible fingertip positions of the proposed structure without any structure limitations are represented as the reachable ROM. The reachable ROM of the proposed structure was compared with the functional ROM. Fingertip positions of functional ROM are obtained by functional ROM of finger joints in Table 1. Fig. 10 shows the comparison between fingertip positions of the functional and reachable ROM with the proposed hand exoskeleton structure. As shown in Fig. 10 (a), the reachable ROM is about 90 % of the functional space, which excluded fingertip positions of very flexed postures.

By adjusting the lengths of links, the reachable ROM of the proposed linkage structure can be increased as shown in Fig. 10 (b) (about 95 % of the functional ROM). But size of the structure increases about 20 mm in height as shown in Fig. 11. The final design was chosen by considering both the ROM and size of the structure. With the final design, the proposed linkage structure can move up to 93° (MCP joint), 89° (PIP joint), and 85° (DIP joint), which are 93 %, 85 %, and 100 % of the normal ROM, respectively.

### 3.4. Analysis of force transmission

In the proposed exoskeleton structure, the generated force by the actuator located at the dorsal side of the hand is transmitted through the exoskeletal structure. How the generated force is

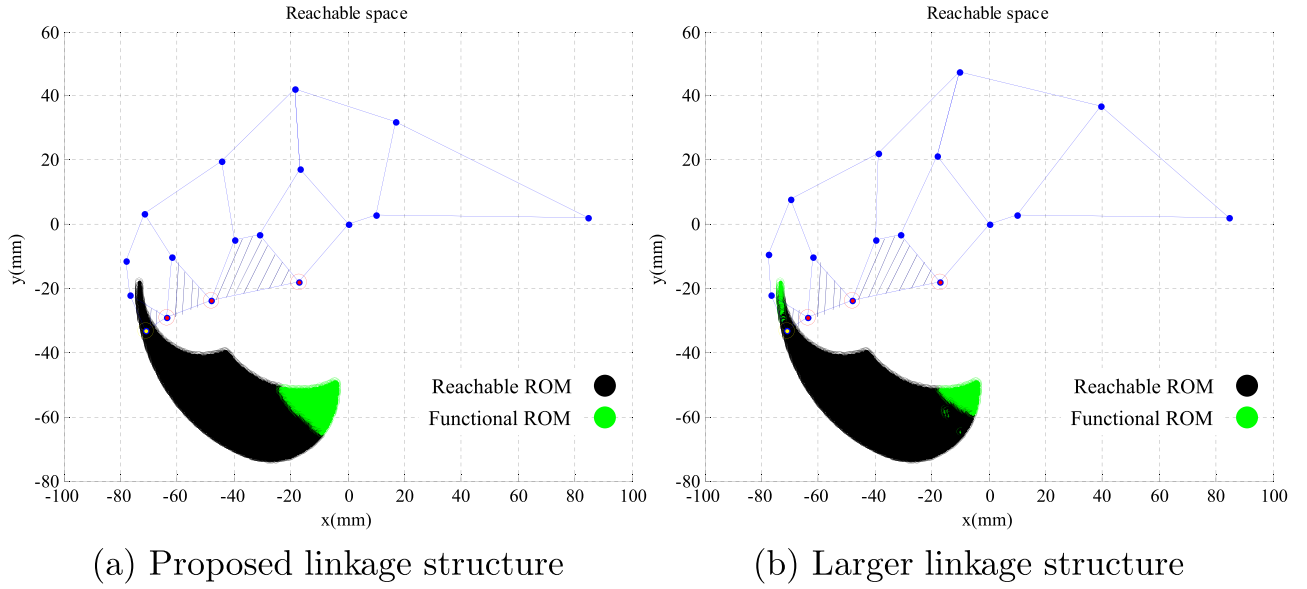


Fig. 10. Comparison of the ROM.

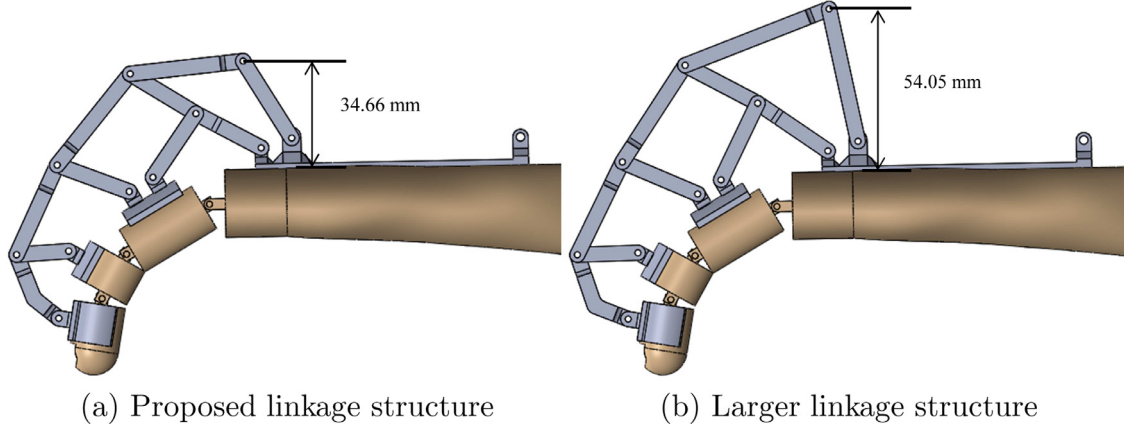


Fig. 11. Comparison of the structure height.

transmitted through the structure to the fingertip is one of important analysis to evaluate the proposed structure.

By assuming a quasi-static situation, the force transmission by the linkage structure is analyzed as shown in Fig. 12. The circles with numbers in Fig. 12(a) represent rotational joints of the linkage structure and the arrows along with the links are the applied force to each joint. As the configuration of the exoskeleton structure was changed according to the finger posture, and the direction and magnitude of the force were calculated by force equilibrium of each joint.

$F$  and  $F_{tip}$  in the figure represent the pulling force by the actuator module and the normal force applied to the fingertip, respectively. We focus on the transmitted force in normal direction at the fingertip because people generally feel normal resistive forces while interacting with objects. The exoskeleton structure contacts with the hand through the parts (4, 9, 12, 16 in Fig. 12(a)), and the transmitted forces to the finger act as the reactive forces from objects at these points (green arrows in Fig. 12(a)). Force equilibrium equations of each joint were formulated using the schematic in Fig. 12(a), for example, as in Fig. 12(b) and represented as following equations:

$$F_{9x} + F_{9y} - F_{10a} - F_{5a} = 0 \quad (14)$$

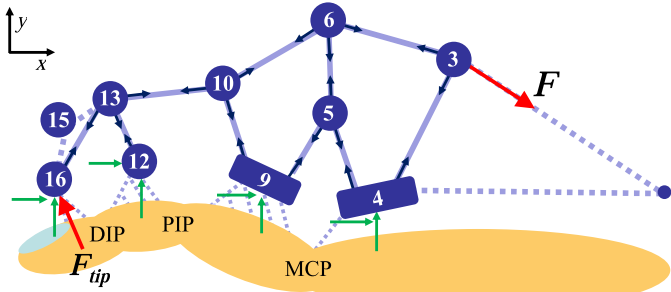
$$F_{10a} + F_{10b} - F_{6b} = 0 \quad (15)$$

$$F_{6a} + F_{6b} - F_{3a} = 0 \quad (16)$$

$$F_{5a} - F_{4a} - F_{6a} = 0 \quad (17)$$

All forces applied to the joints were investigated by force equilibrium equations and the normal force applied to the fingertip  $F_{tip}$  was calculated. The simulated angle ranges of joints are same with the ROM from Table 1 used in the kinematic analysis. The movement of DIP joint is highly dependent on the PIP joint in general flexion/extension motions and its angle is about 2/3 of the PIP joint angle [14]. The generated force by the actuator ( $F$  in Fig. 12(a)) was set as 3 N in this simulation.

Fig. 13 shows the simulation results about the transmitted force to the fingertip. The DIP joint angles were changed according to the PIP joint angles although the DIP joint angles were not specified. The white region is the unreachable ROM of the proposed structure and the transmitted forces to the fingertip were obtained. The amount of transmitted force to the fingertip,  $F_{tip}$ , depends on the finger joint angles; it is decreased as the finger flexed. This



(a) The whole structure

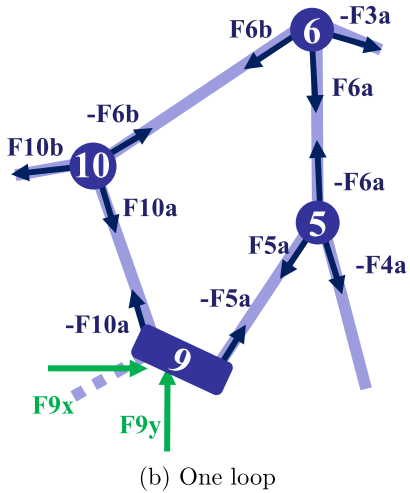


Fig. 12. Force transmission analysis.

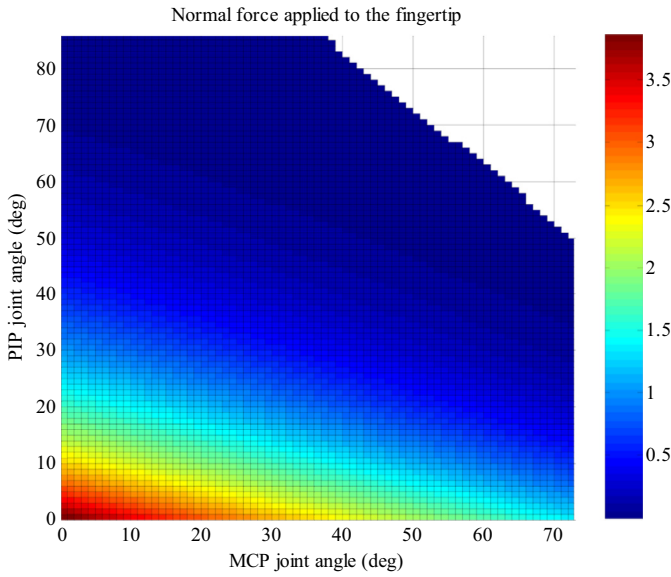


Fig. 13. Transmitted force to the fingertip (simulation).

is because the normal direction of the fingertip is changed by the joint angles. If the angle of the PIP joint is zero, the force at the fingertip is decreased from maximum 3.5 N to 1.5 N according to the change of the MCP joint angle. The force at the fingertip is also decreased by the PIP joint angle. The decreased amount of the transmitted force by PIP joint angle is larger than that by MCP joint angle because the DIP joint is moved with the PIP joint.

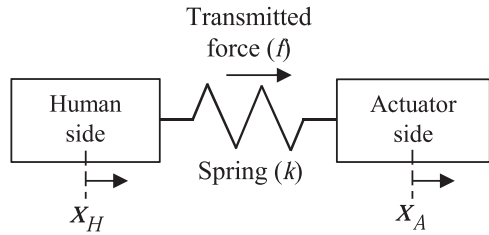


Fig. 14. Schematic of the series elastic actuator (SEA) mechanism.

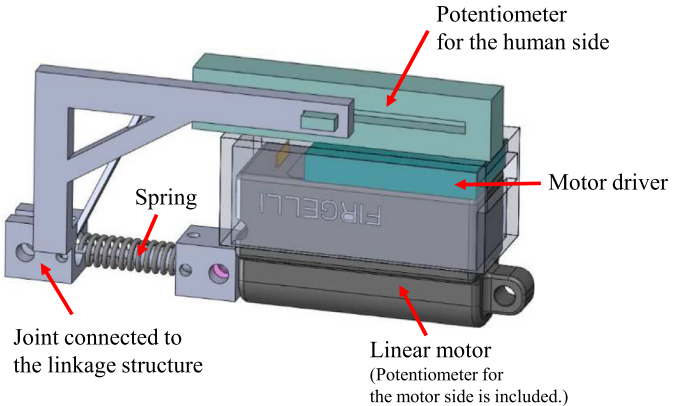


Fig. 15. Design of the actuator module.

#### 4. Design of a compact actuator module

##### 4.1. Series elastic actuator (SEA) mechanism

To achieve active interaction with the finger motion, force mode control is required with real-time force measurements. However, a conventional force sensor may not be appropriate for the hand exoskeleton system due to its bulky size and heavy weight. In the proposed system, a series elastic actuator (SEA) mechanism is used for the compact design and accurate force control.

The SEA mechanism has been widely used for force mode control of the physical human-robot interaction systems [1–3,16,18,19]. In this mechanism, the force generated by an actuator is transmitted via an elastic element, i.e., a spring, which is installed between the human side and the actuator. Fig. 14 shows a schematic diagram of the SEA mechanism. The transmitted force,  $f$ , is controlled by the deflection of the spring as follows:

$$f = k(x_A - x_H) \quad (18)$$

where  $k$  is the spring constant, and  $x_A$  and  $x_H$  are the positions of the actuator and human side, respectively. The desired actuator position,  $x_{Ad}$ , is determined by the measured human joint motion and the given desired force,  $f_d$ , as follows:

$$x_{Ad} = \frac{f_d}{k} + x_H \quad (19)$$

By controlling the motor to the desired motor position, the desired force can be generated.

Design of the actuator module using the SEA mechanism is shown in Fig. 15. The position of the linkage structure was measured by a potentiometer of the human side, and that of the actuator was measured by an embedded potentiometer in the linear motor. Because the transmitted force was applied and measured using linear spring deflection, the hand exoskeleton system did not require a conventional force sensor. This mechanism makes the design of the actuator module more compact; additionally, the sensitivity of the force measurement could be adjusted easily by changing the spring constant.

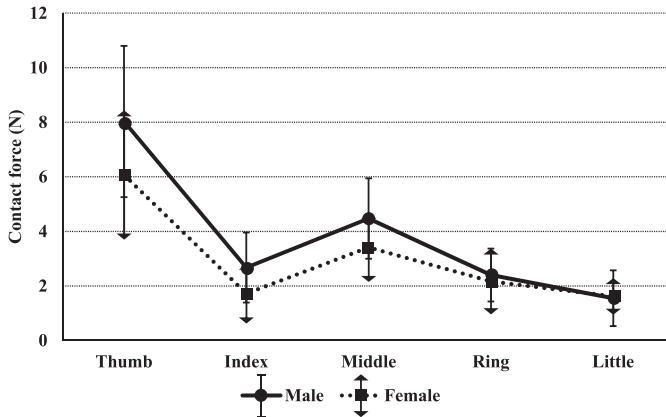


**Fig. 16.** Maximum grasp force of each finger.

**Table 2**  
Parameters of the spring design.

Modulus of rigidity	$G$ (kgf/mm <sup>2</sup> )	7500
Diameter of a spring wire	$d$ (mm)	0.6
Mean diameter of a spring	$D$ (mm)	6.5
Number of turns	$n$	10
Spring constant	$k$ (N/mm)	0.434

#### 4.2. Design of the actuator module

To examine the interactive force to manipulate objects, the contact forces at the fingertip in manipulating objects were measured. The film-type pressure sensors (Tekscan grip system) were used for measuring contact forces. The sensors were attached at the palm side of the hand and measured the grip force by fingertips. The subject wore the glove and grasped middle size cup (diameter: 6.4 cm) gently for 5 s just before lifting up the cup by using fingertips only. After the trial, the subject rested some minutes and repeated the grasp. The participants are seven healthy persons (four males, three females, age:  $24 \pm 4.3$ ) without any known motor diseases. Each person had five trials and the maximum contact forces for all trials were averaged.

The experimental results are given in Fig. 16; the solid and dotted lines represent the average values for the males and females, respectively. The grip force of the thumb was largest for all participants, about 8 N for males and about 6 N for females. Regarding the required linear stroke of a motor, the simulation result in Fig. 10(a) verified that about 20 mm linear motion was enough to achieve the functional ROM for daily activities. Therefore, a linear motor with a 20 mm stroke and 9 N maximum force (Firgelli PQ12) was selected as the main actuator.

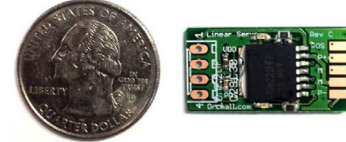
The linear spring plays an important role in the proposed force-controllable actuator module because the amount of force is controlled by spring deflection. It is known that the average force resolution of the PIP and MCP joints is about 0.3 N [22]. If it is assumed that the actuator can be controlled with less than 1 mm position error, then a spring constant of 0.3–0.5 N/mm may be sufficient for the resolution of the finger. Considering the size of the linkage structure and the linear motor, the design parameters were determined as in Table 2, and the spring constant was calculated as 0.434 N/mm by the following equation [5]:

$$k = \frac{Gd^4}{8D^3n} \quad (20)$$

where  $G$  is the modulus of rigidity,  $d$  is the diameter of a spring wire,  $D$  is the mean diameter of a spring, and  $n$  is the number of active coils.



(a) Manufactured actuator module



(b) Manually designed motor driver

**Fig. 17.** The actuator module.

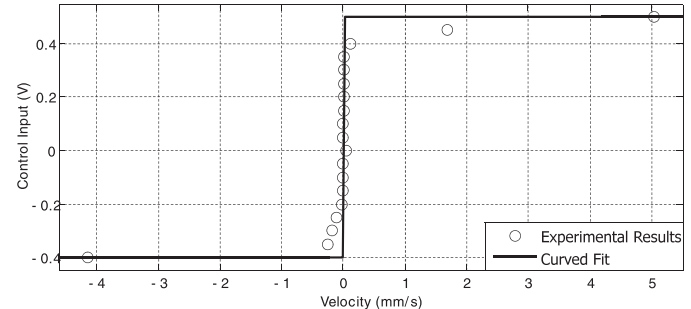


**Fig. 18.** Friction identification.

The compact actuator module was manufactured as shown in Fig. 17(a). The driver was manually designed as shown in Fig. 17(b). It was  $27 \times 14 \times 4$  mm, small enough to be attached to the top of the linear motor. The motor driver was attached to the top of the motor and hidden by a manufactured cover to protect electronic cables. The potentiometer to measure the finger motion was placed on top of the actuator module due to the limited space available. The structure was manufactured with nylon material using rapid prototyping technology. Its size was about  $18 \times 77 \times 36$  mm, and its weight was 30 g.

#### 5. Force control of the actuator module

##### 5.1. Linearized model by friction compensation

The electric motor in the actuator module is used with a gear reducer to adjust the force or speed range as desired. The gear reducer amplifies the output force, but it also amplifies friction of the motor itself, which is the dominant nonlinearity of the geared motor. In this paper, the linear plant model was obtained by friction compensation to achieve improved control performance.

To compensate friction of the motor, the friction model was experimentally identified. Fig. 18 shows the experimentally obtained control inputs at various velocities of the motor. A signum function could be included to the friction model, but the signum function may cause undesired vibration when the actuator velocity is near zero. To eliminate such vibration, the input voltage for friction compensation was set to zero when the actuator velocity is near zero. Thus, the control voltage for the friction compensation,

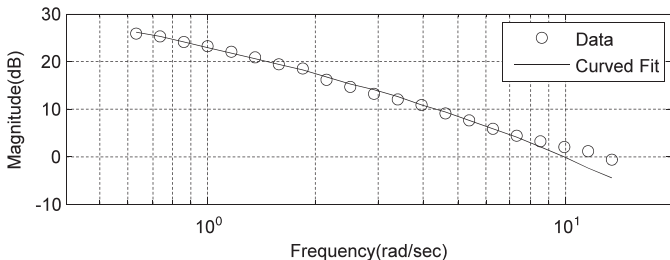


**Fig. 19.** Frequency response of the system with friction compensation.

$V_{fric}$ , was generated as follows:

$$V_{fric} = a + b \cdot \text{sgn}^*(v_A) \quad (21)$$

where  $v_A$  is the velocity of actuator and  $\text{sgn}^*(v_A)$  was defined as follows:

$$\text{sgn}^*(v_A) = \begin{cases} -1, & v_A < -\epsilon \\ -a/b, & -\epsilon \leq v_A < \epsilon \\ 1, & v_A \geq \epsilon \end{cases} \quad (22)$$

The actuator velocity range which had the input voltage as zero ( $\epsilon$  in 22) was determined experimentally considering the noise magnitude. Coefficients  $a$  and  $b$  in (21) represent bias and Coulomb friction, respectively. By fitting the experimental data, the parameters were identified as  $a = 0.05$ ,  $b = 0.45$ , and  $\epsilon$  was set to 0.3. Fig. 19 shows the experimentally obtained frequency responses by sweeping sinusoidal signals to the plant with the friction compensation. The linearized model was identified as follows:

$$P(s) = \frac{124.7}{s^2 + 8.527 s + 3.708} \quad (23)$$

## 5.2. Control algorithms for accurate tracking with enhanced robustness

A PD controller was applied for the actuator module as a tracking controller. The PD control gains were optimally obtained by applying a linear quadratic (LQ) method. The cost function to be minimized in the LQ method was,

$$J = \int_0^\infty \{e^T(t)Qe(t) + u^T(t)Ru(t)\}dt \quad (24)$$

where  $e$  is the tracking error,  $u$  accounts for the control input,  $Q$  and  $R$  are weighting factors for system states and control input. The weighting factor for system states  $Q$  is a  $2 \times 2$  matrix. The

(1,1) and (2,2) elements in the matrix are the weighting factors for position tracking error and for velocity tracking error, respectively. The actuator in the proposed system should be precisely position-controlled for SEA mechanism so the weighting factor for position tracking error was set to be larger than that for velocity tracking error. The weighting factor for control input  $R$  was determined not to saturate the control input while the actuator was controlled well. In this paper, the weighting factors for system states and control input were determined by try and error method.  $Q$  and  $R$  were selected as  $[10; 0.00001]^T$  and 0.2, respectively.

The optimal PD controller with the linearized plant may work well as a tracking controller, but the modeling uncertainties, especially introduced by the interaction with finger motions, deteriorates the control performance. To enhance the robustness against the modeling uncertainties, the disturbance observer (DOB), which is one of the representative robust control algorithms, was applied for the system. By extracting the estimated disturbance, the disturbance or modeling uncertainties can be compensated. Considering the specification of the motor and the human motion speed, the  $Q$  filter in the DOB was implemented as a second order low-pass filter with cut-off frequency of 3 Hz.

Now the block diagram of the overall control algorithms is depicted in Fig. 20. From the desired force,  $f_d$ , the desired motor position,  $x_{Md}$  is calculated by (19) ('Position Conversion' box in Fig. 20). For the accurate position control, the LQ tuned PD controller ('C' in Fig. 20) is applied as an outer loop. The actual plant (a geared linear motor, 'P' in Fig. 20), is linearized by friction compensation, and the remaining or introduced uncertainties are dealt with the DOB. The actual motor position,  $x_M$ , is converted to the applied force,  $f$ , by (18) ('Force Conversion' box in Fig. 20).

To verify the force control performance of the proposed algorithm, generating the desired force with arbitrary finger motion was tested. The desired force was set to a sinusoidal signal, and the human side motion,  $x_H$  in (18) and (19), was given as an arbitrary finger motion. The experimental results are shown in the Fig. 21. Fig. 21 (a) shows the position tracking performance of the motor. Note that the desired motor position was determined by the arbitrary finger motion in real-time by (19), and the motor was able to track it well. With the arbitrary finger motions, the desired force was generated accurately as shown in Fig. 21 (b) and (c). The root-mean-squared error (RMSE) was 0.09 N and the maximum error was 0.27 N, which was smaller than the force resolution of the finger joint [22].

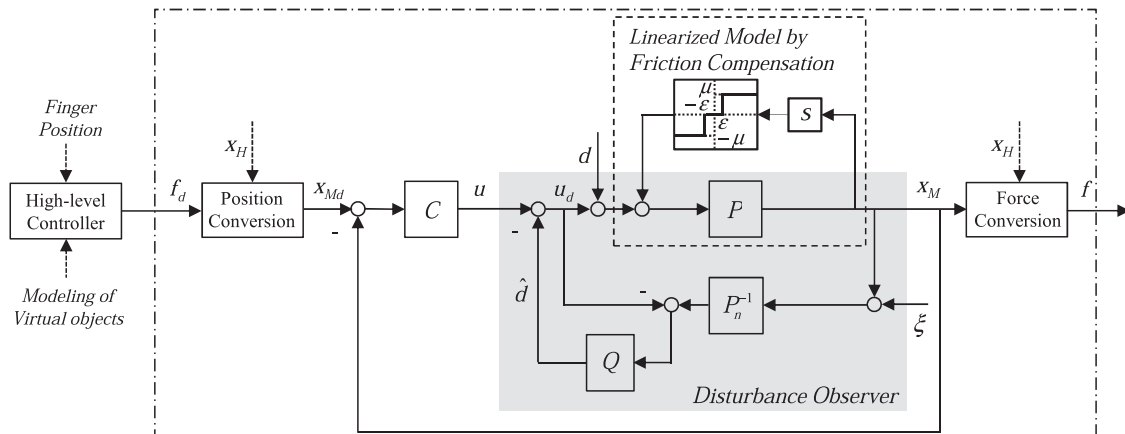


**Fig. 20.** Overall structure of the proposed controller for the compact actuator module ( $P$ : plant,  $P_n$ : nominal model of  $P$ ,  $Q$ :  $Q$  filter in the DOB,  $C$ : controller,  $f_d/f$ : desired/measured force,  $x_{Md}/x_M$ : desired/measured motor position,  $x_H$ : finger position,  $d/d\hat{d}$ : external/estimated disturbance,  $u$ : control input,  $u_d$ : control input in the DOB,  $\xi$ : noise).

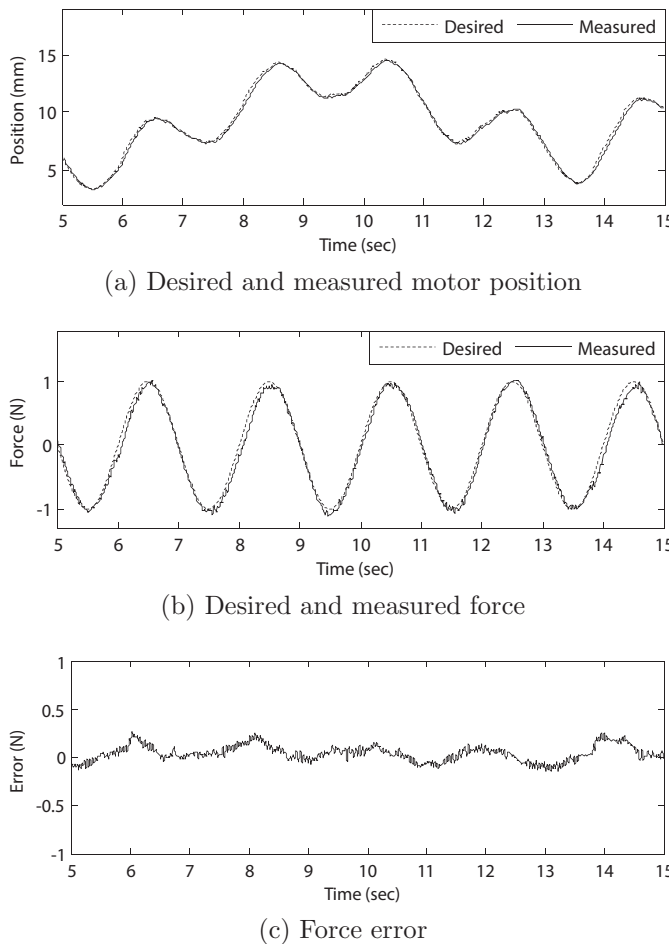


**Fig. 21.** Force control performance with arbitrary finger motion.

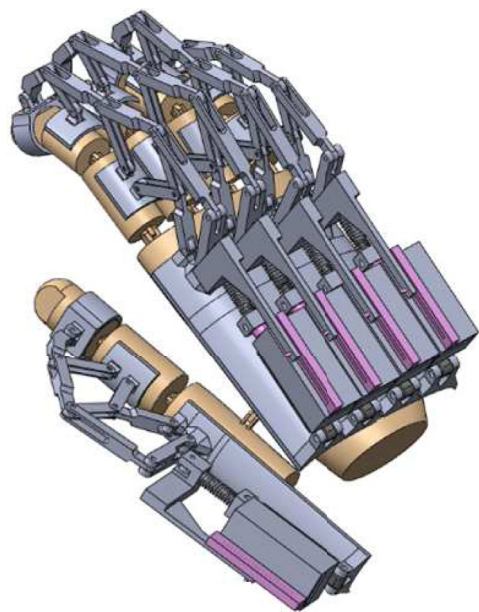
## 6. Implementation of the wearable and force-controllable hand exoskeleton

### 6.1. Integration of the system

The proposed exoskeleton structure and actuator modules were integrated as shown in Fig. 22(a), and manufactured as shown in Fig. 22(b). The structure was attached to a glove for easy wearing. The size and weight were  $88 \times 230 \times 83$  mm and 298 g, respectively. The transmitted force to each finger was controlled by one actuator and all actuator modules were put on the back of the hand for the unconstrained hand movement. Although it includes five actuator modules, the size and weight are quite small to move the user's arm naturally. Although all required equipments except batteries were placed on the back of the hand, the proposed hand exoskeleton shows the compact size and wearable shape.

### 6.2. Experimental results on force transmission

Applying the force to the fingertip, which is one of the important goals of the proposed system, was tested with the prototype of hand exoskeleton system. The fingertip part of the index finger was modified to install a load cell(CLS-20NA, TML [24]) at the bottom of the fingertip of exoskeleton as shown in Fig. 23(a). It measured the normal force at the fingertip when the structure was pulled up by the actuator module. Fig. 23(b) shows the experimental setup: a user worn the hand exoskeleton was asked to have three finger postures ((DIP, PIP, MCP): (0, 0, 30), (0, 0, 45), (10, 15, 30) deg), and 3 N force was applied by the actuator module. The



**(a)** Design of the hand exoskeleton

**(b)** Prototype of the hand exoskeleton

**Fig. 22.** The proposed hand exoskeleton system.

finger joint angles were measured by a goniometer. The experiment was conducted 10 times for each posture, and the force at the fingertip was measured.

The experimental results are summarized in Fig. 24; the solid dots and dashed lines represent average and standard deviation, respectively. As the simulation results in Section 3.4, the force transmission ratio is decreased as the finger is flexed, which is explained by the same reason of the simulation. The amount of the transmitted forces were smaller than those of simulation, which may be caused by the imperfect hardware manufacturing such as misalignment of joint or friction. But, based on the simulation and experimental results, the amount of transmitted force to the fingertip can be changed by adjusting the generated force at the actuator module.

## 7. Conclusion and future work

In this paper, a wearable and force-controllable hand exoskeleton system was designed and experimentally verified. The exoskeleton structure inspired by finger anatomy was designed with consideration for DOF and ROM. The reachable ROM was investigated by kinematically analyzing the proposed structure and sat-

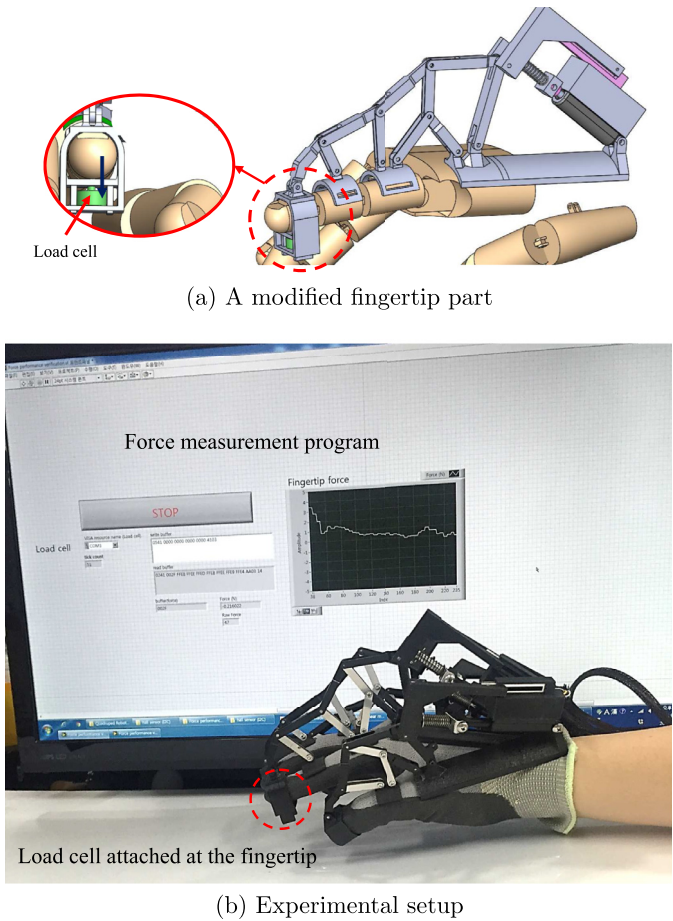


**Fig. 23.** Force transmission experiment.

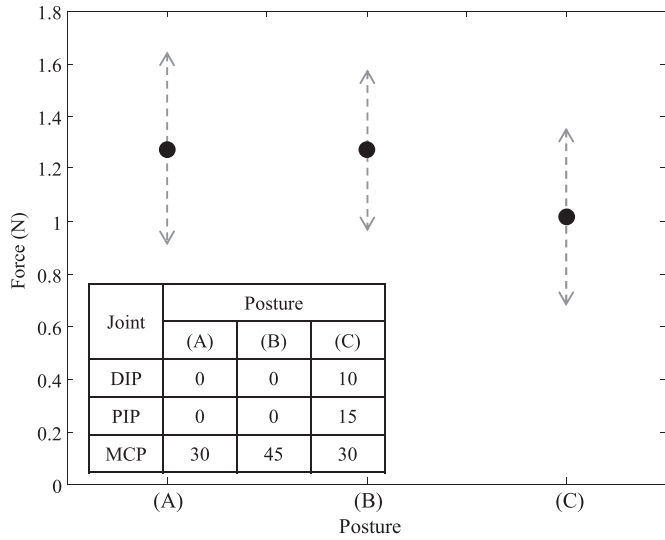


**Fig. 24.** Normal force at the fingertip in experiment.

isified 90% of the functional ROM. For the actuator part, a series elastic actuator (SEA) mechanism was applied. The actuator modules were composed of an actuator, a spring, a human side potentiometer for force mode control. To decide the maximum motor force, the experiments for measuring resistive force from the object were conducted. The selected motor was linearized by the friction compensation and the robust control algorithm was applied to achieve accurate force mode control. The actuator modules were so

compact that they could be directly attached to the hand exoskeleton structure, which allows the user to move the hand naturally. The desired force was generated accurately in the actuator module even with arbitrary finger motions, but actually transmitted force to the fingertip was smaller than the generated one due to the drastic change in the normal direction of the fingertip as the finger is flexed. But the amount of transmitted force to the fingertip can be changed by adjusting the generated force of the actuator module based on the simulation and experimental results.

As a future work, the developed hand exoskeleton system will be combined with a finger motion measurement system. Also, the exoskeleton structure with more degrees of freedom (DOFs) will be developed to include adduction and abduction motions. Thus, it will be utilized as a general haptic system to interact with virtual environments.

### Acknowledgment

This work was supported by the Global Frontier R&D Program on < Human-centered Interaction for Coexistence> funded by the National Research Foundation of Korea grant funded by the Korean Government(MSIP) (NRF-2012M3A6A3056354). Preliminary versions of this paper were presented at the World Congress of the International Federation of Automatic Control (IFAC WC) 2014 and IEEE International Conference on Robotics and Automation (ICRA) 2015.

### References

- Bae J, Kong K, Tomizuka M. Gait phase-based control for a rotary series elastic actuator assisting the knee joint. *ASME J Med Dev* 2011;5: 031010-1–6.
- Bae J, Tomizuka M. A gait rehabilitation strategy inspired by an iterative learning algorithm. *Mechatronics* 2012;22:213–21.
- Bae J, Zhang W, Tomizuka M. Network-based rehabilitation system for improved mobility and tele-rehabilitation. *IEEE Trans Control Syst Technol* 2013;21:1980–7.
- Banala SK, Kim SH, Agrawal SK, Scholz JP. Robot assisted gait training with active leg exoskeleton (ALEX). *IEEE Trans Neural Syst Rehabil Eng* 2009;17:2–8.
- Budynas RG, Nisbett JK. Shigley's mechanical engineering design. McGraw-Hill; 2011.
- Chiri A, Vitiello N, Giovacchini F, Roccella S, Vecchi F, Carrozza MC. Mechatronic design and characterization of the index finger module of a hand exoskeleton for post-stroke rehabilitation. *IEEE/ASME Trans Mechatron* 2012;17:884–94.
- Cyber Glove Systems. Cyber Grasp. 2016. <http://www.cyberglovesystems.com/>.
- FESTO. Exo-Hand. 2016. <http://www.festo.com/>.
- Fontana M, Dettori A, Salsedo F, Bergamasco M. Mechanical design of a novel hand exoskeleton for accurate force displaying. *IEEE Int Conf Rob Autom (ICRA) 2009*:1704–9.
- Hume M, Gellman H, McKellop H, Brumfield R. Functional range of motion of the joints of the hand. *J Hand Surg Am* 1990;15(2):240–3.
- In H, Cho K, Kim K, Lee B. Jointless structure and under-actuation mechanism for compact hand exoskeleton. In: *IEEE International Conference on Rehabilitation Robotics (ICORR)*; 2011. p. 1–6.
- Iqbal J, Ahmad O, Malik A. Hexosys ii-towards realization of light mass robotics for the hand. In: *IEEE international multtopic conference (INMIC)*; 2011. p. 115–19.
- Jonathan Engel JC, Liu C. Development of polyimide flexible tactile sensor skin. *J Micromech Microeng* 2003;13:559–66.
- Kamper D, Cruz E, Siegel M. Stereotypical fingertip trajectories during grasp. *J Neurophysiol* 2003;6:3702–3710.
- Neumann D, Rowan E. Kinesiology of the musculoskeletal system: foundations for physical rehabilitation. Mosby Philadelphia; 2002.
- Paluska D, Herr H. Series elasticity and actuator power output. *IEEE Int Conf Rob Autom (ICRA) 2006*:1830–3.
- Perry JC, Rosen J, Burns S. Upper-limb powered exoskeleton design. *IEEE/ASME Trans Mechatron* 2007;12:408–17.
- Pratt G, Williamson M. Series elastic actuators. *IEEE/RSJ Int Conf Intell Rob Syst (IROS) 1995*:399–406.
- Pratt J, Krupp B, Morse C. Series elastic actuators for high fidelity force control. *Int J Ind Robot* 2002;29:234–41.
- Riener R, Lunenburger L, Jezernik S, Anderschitz M, Colombo G, Dietz V. Patient-cooperative strategies for robot-aided treadmill training: first experimental results. *IEEE Trans Neural Syst Rehabil Eng* 2005;13:380–94.
- Ruth D, McCarthy J. The design of spherical 4r linkages for four specified orientations. *Mech Mach Theory* 1999;34:677–92.
- Tan HZ, Srinivasan MA, Eberman B, Cheng B. Human factors for the design of force-reflecting haptic interfaces. *Dyn Syst Control* 1994;55:353–9.

- [23] Tian Y, Shirinzadeh B, Zhang D. Stiffness estimation of the flexure-based five-bar micro-manipulator. In: Intl. conf. on control, automation, robotics and vision; 2008. p. 599–604.
- [24] TML. CLS-20NA. 2016. <http://www.tml.jp/>.
- [25] Veneman JF, Kruidhof R, Hekman EE, Ekkelinkamp R, Asseldonk EHV, van der Kooij H. Design and evaluation of the LOPES exoskeleton robot for interactive gait rehabilitation. *IEEE Trans Neural Syst Rehabil Eng* 2007;15:379–86.
- [26] Zoss A, Kazerooni H, Chu A. Biomechanical design of the berkeley lower extremity exoskeleton (BLEEX). *IEEE/ASME Trans Mechatron* 2006;11:128–38.